Journal of Dental Sciences 19 (2024) 1653–1666

Available online at www.sciencedirect.com

ScienceDirect

journal homepage: www.e-jds.com

Mineral trioxide aggregate in membrane form as a barrier membrane in guided bone regeneration

Min-Yong Lee [a], Hi-Won Yoon [b], Si-Yoon Lee [c], Kwang-Mahn Kim [a], Su-Jung Shin [b], Jae-Sung Kwon [a,d*]

[a] *Department and Research Institute of Dental Biomaterials and Bioengineering, Yonsei University College of Dentistry, Seoul, South Korea*
[b] *Department of Conservative Dentistry, Gangnam Severance Hospital, Yonsei University College of Dentistry, Seoul, South Korea*
[c] *Department of Biology, New York University, New York, NY, USA*
[d] *BK21 FOUR Project, Yonsei University College of Dentistry, Seoul, South Korea*

Received 24 October 2023; Final revision received 27 November 2023
Available online 6 December 2023

KEYWORDS
Mineral trioxide aggregate;
Polycaprolactone;
Electrospinning;
Barrier membrane;
Guided bone regeneration

Abstract *Background/purpose:* In the field of conservative dentistry and endodontics, mineral trioxide aggregate (MTA), commonly used, possesses advantages such as biocompatibility, antimicrobial properties and osteogenic potential. This study investigated the feasibility of utilizing membrane form mineral trioxide aggregate (MTA) as a barrier membrane in guided bone regeneration (GBR) procedures.
Materials and methods: Membranes were electrospun from three different formulations: 15 w/v% Polycaprolactone (PCL), 13 w/v% PCL + 2 w/v% MTA (2MTA), and 11 w/v% PCL + 4 w/v% MTA (4MTA). Physicochemical and mechanical properties of the electrospun membrane were compared, encompassing parameters such as surface morphology, fiber diameter distribution, chemical composition, phase identification, tensile stress, pH variation, and water contact angle. Moreover, the antimicrobial properties against of the electrospun membranes were assessed through direct exposure to *streptococcus aureus* (*S. aureus*) and *candida albicans* (*C. albicans*). Additionally, on the 7th day, biocompatibility and cell attachment were investigated with respect to L929 (fibroblast) and MC3T3 (pre-osteoblast) cells. Inhibition of L929 cell infiltration and the expression of osteogenic related genes including osteocalcin (OCN), alkaline phosphatase (ALP), and runt related transcription factor 2 (RUNX2) in MC3T3 cells on 7th and 14th days were also investigated.

* Corresponding author. Department and Research Institute of Dental Biomaterial and Bioengineering, Yonsei University College of Dentistry, 50-1 Yonsei-ro, Seodamun-gu, Seoul, 03722, South Korea.
E-mail address: JKWON@yuhs.ac (J.-S. Kwon).

https://doi.org/10.1016/j.jds.2023.11.021

Results: PCL, 2MTA, and 4MTA exhibited no statistically differences in fiber diameter distribution and tensile stress. However, as the MTA content increased, wettability and pH also increased. Due to the elevated pH, 4MTA demonstrated the lowest viability *S.aureus* and *C.albicans*. All membranes were highly biocompatibility and promoted cell attachment, while effectively preventing L929 cell infiltration. Lastly 4MTA showed increase in OCN, ALP, and RUNX2 expression on both 7th and 14th day.
Conclusion: The membrane form MTA possessed characteristics essential for a novel barrier membrane.

Introduction

In the field of conservative dentistry and endodontics, mineral trioxide aggregate (MTA), commonly used, possesses advantages such as biocompatibility, antimicrobial properties and osteogenic potential.[1–3] However, conventional MTA was in powder form, requiring manual mixing, which presented a drawback. Recently, various manufacturers have introduced premixed paste forms of MTA for convenience. Currently, premixed MTA is recognized for its performance comparable to powder MTA.[4,5] In this study, we aim to further modify the morphology of MTA.

Barrier membranes used in guided bone regeneration (GBR) play a crucial role in physically covering bone defects to facilitate regeneration.[6] The primary goal of a barrier membrane is to prevent fibroblast infiltration into the bone defect area.[7] If it also possesses additional feature such as antimicrobial properties, improved osteoblast proliferation, biodegradable, and promotion of cell attachment, it can be considered a novel barrier membrane.[8,9] The most commonly used type of barrier membrane currently is the xenogeneic membrane, primarily composed of collagen. However, it has drawbacks such as high cost and lack of antimicrobial properties. Therefore, there have been many attempts to create synthetic polymer barrier membranes with the addition of specific substances or multi-layered structure.[10,11] Fortunately, The intrinsic characteristics of MTA meet the criteria that a novel barrier membrane should possess. However, due to its powder or paste morphology, MTA needs to be transformed into a membrane form using a new manufacturing method.

Porous and non-woven membrane fabricated using electrospinning mimic the appearance of the natural extracellular matrix (ECM).[12] Polycaprolactone (PCL) is a representative polymer used in electrospinning, known for its high biocompatibility and ease of blending with bioceramic materials.[13] However, the limited utilization of PCL as a barrier membrane, despite its various advantages, is attributed to its hydrophobic characteristics and low biological activity.[14] If MTA is incorporated in a high concentration with PCL to create a membrane that mimics the ECM, it has the potential to improve the disadvantages of PCL. Particularly, noteworthy in this study is the fact that it represents the initial attempts to fabricate a barrier membrane using electrospinning by combining PCL and paste form MTA.

The purpose of this experiment was to fabricate a membrane form MTA that could replace the collagen membrane currently being used. There are three null hypotheses in this context. Firstly, as the MTA content increases in electrospun membranes, there would be no significant decrease in the water contact angle. Secondly, despite an increase in MTA content in electrospun membranes, the viability of *Staphylococcus aureus* (*S. aureus*) and *Candida albicans* (*C. albicans*), which are in direct contact with the membrane, would not show a significant decrease. Lastly, even when cells are cultured on the membrane with higher MTA content, there would be no significant increase in expression of osteogenic genes.

Materials and methods

Fabrication of mineral trioxide aggregate embedded electrospun polycaprolactone membrane

The experiment involved the preparation of a solution comprising Polycaprolactone (PCL; M_w: 80,000, Sigma-Aldrich, St. Louis, MO, USA) and Endocem MTA Premixed Regular (MTA; Maruchi, Wonju, Kwangwon-do, Korea) in a solvent blend of chloroform (CF; Sigma-Aldrich) and N,N-Dimetylformamide (DMF; Tokyo Chemical Industry, Chuo-ku, Japan). The required amount of MTA and PCL was dispersed within the solvent and stirred magnetically at a 60 °C overnight (Table 1). This prepared solution was then loaded into a 5 mL syringe (KOVAX, Seoul, Korea) equipped with a 23-gauge metal nozzle (NanoNC, Seoul, Korea). The flow rate of the polymer solution was maintained at 1 mL/h and controlled by an

Table 1 Preparation of electrospun membrane.

Groups	Solvent	Amount of PCL and MTA
PCL	10 mL (9 mL CF + 1 mL DMF)	1.5 g PCL (15 w/v%)
2MTA	10 mL (9 mL CF + 1 mL DMF)	1.3 g PCL (13 w/v%) + 0.2 g MTA (2 w/v%)
4MTA	10 mL (9 mL CF + 1 mL DMF)	1.1 g PCL (11 w/v%) + 0.4 g MTA (4 w/v%)

CF; Chloroform, DMF; N,N-Dimetylformamide, MTA; Mineral trioxide aggregate, PCL; Polycaprolactone.

electrospinning machine (ESR200R2D, NanoNC). An electrospinning voltage of 15 kV was applied to the needle at 20 °C temperature, with a 10 cm distance between the needle tip and the stationary collector. Electrospun PCL membranes were fabricated, with two variants containing 2 w/v% and 4w/v% of MTA, designed as 2MTA and 4MTA respectively. The fabricated specimen had dimensions of 60 mm in length, 20 mm in width, and 0.4 mm in thickness.

Evaluation of physical property of mineral trioxide aggregatre

In order to prevent the hydration and agglomeration of MTA, MTA was diluted with 99 % ethanol (Sigma-Aldrich) and sonicated for 10 min. Subsequently, the mixture was deposited onto a carbon grid and dried overnight. The morphology and particle dimensions of MTA were assessed through transmission electron microscopy (TEM; JEOL-2100Puls, Akishima, Japan) at a magnification of 15,000x.

Evaluation of morphology, composition, and phase state of electrospun membrane

Assessment of morphology of electrospun membrane

A comparative analysis was conducted to assess the morphology of both the front and back sides of each electrospun membrane. The front side refers to the side of the membrane facing the direction of the metal nozzles, while the back side refers to the side facing the collector. The morphology of the electrospun membrane was examined using a scanning electron microscope (SEM; IT-500HR, JEOL), and the diameter distribution of fiber was analyzed using image visualization software, Image J (National Institute of Health, Stapleton, NY, USA).

Evaluation of the chemical composition and phase state of the electrospun membrane

The four elemental composition of each membrane was analyzed using energy-dispersive X-ray spectroscopy (EDS, JEOL) at a magnification of 1,000x. The four elements were carbon (C), oxygen (O), calcium (Ca), and zirconium (Zr). The microstructure of the electrospun membrane was further investigated using X-ray diffraction (XRD; Ultimate IV, Rigaku, Akishima, Japan) with Cu K α radiation source ($\lambda = 1.5406$ Å). XRD patterns were recorded within the 2 θ range 20–70° at a scanning speed of 1°/min. The operating conditions included a voltage was 40 kV, a current of 30 mA and a step size of 0.02°.

Physicochemical properties of mineral trioxide aggregate embedded electrospun polycaprolactone membrane

Tensile strength test

Rectangular samples of the electrospun membrane were created by cutting them, resulting in dimensions of 20 × 15 mm^2, following the conventional GBR membrane products. The thickness of each sample was measured using a vernier caliper (Mitutoyo, Takatsu-ku, Japan), which measured 0.4 mm. Tensile strength assessments were carried out using a universal testing machine (UTM; Instron 5942, Norwood, MA, USA). All samples were securely held between holders, maintaining a 10 mm separation. The tensile tests were executed at a constant rate of 5 mm/min. Experimental values were automatically calculated through the Instron software (Bluehill 2, Elancourt, France).

pH variance test

To assess pH changes, each membrane was cut into dimensions of 20 × 15 mm^2 (0.015 g). These membranes were then immersed in 5 mL of deionized water (dH_2O) and gently agitated at 120 rpm at a temperature of 37 °C. The pH of the solution was measured at intervals of 0, 1, 2, 3, 4, 5, 6, and 24 h, using a pH meter (Orion 4 star; Thermo Fisher Scientific, Waltham, MA, USA). Each pH measurement was conducted three times for accuracy.

Water contact angle test

To evaluate the wettability of the electrospun membranes, a static contact angle analyzer (Smartdrop lite; Femtobiomed, Seongnam, Korea) was employed. Approximately 5 μ L of deionized water was dispensed onto each dried sample using a microtip, and the resulting contact angle on each sample's surface was analyzed and computed. Both the front and back sides of each membrane underwent five measurement.

Evaluation of antimicrobial effect

Each sample was positioned in a 12-well microplate (SPL Life Sceince-Co., Pocheon, Gyeonggi-do, Korea) and subjected to UV sterilization for 30 min. Subsequently. 100 μL of suspension containing *S.aureus* and *C.albicans,* each with an optical density (OD) of 0.1 at 600 nm, was inoculated onto each membrane. The 12-well microplate was then incubated for 4 h at 37 °C. Following incubation, 1 mL of phosphate-buffered saline (PBS; Gibco, Gand Island, NY, USA) was added to each well and gently pipetted for 1 min. The PBS-diluted microbial suspension and membrane contents were transferred to a 15 mL conical tube. This mixture was vortexing for 20 s to ensure complete detachment of microbial substance from the membrane. Next, 100 μL of this solution was aliquoted into a 96-well plate, and 10 μL of a 0.5 mg/mL 3-(4,5-demethylthiazol-2-yl)-2,5-diphenyltetrazolium bromide (MTT; Sigma-Aldrich) solution was added. We conducted a bacteria and fungi viability test using the MTT assay, referencing previous studies.[15–17] This mixture was incubated for 1 h. After incubation, 10 μL of dimethyl sulfoxide (DMSO; Sigma-Aldrich) was added into each well. Finally, the 96-well plate was gently agitated for 10 min and the absorbance was analyzed at 570 nm using a microplate spectrophotometer (Epoch, Biotek, Winooski, VT, USA). This procedure was replicated three times for each sample. Bacterial and fungal viability (%) was determined using Equation (1), where Exp, represented the absorbance of *S.aureus* or *C.albicans* and MTT solution. Blank represented the absorbance of the MTT solution without microorganisms. Control represented the absorbance of microorganisms and the MTT solution that did not come into contact with membranes.

$$\text{Viability (\%)} = [(\text{Exp} - \text{Blank}) / (\text{Control} - \text{Blank})] \times 100 \quad (1)$$

Live/dead cell viability assay

To culture L929 (fibroblast) and MC3T3 cells (pre-osteoblast), α-minimum essential medium (Gibco) growth medium was used and supplemented with 10 % fetal bovine serum (FBS) (Gibco) and 1 % antibiotic-antimycotic (Gibco).The procedure involved placing each sample in a12-well microplate and subjected them to UV sterilization for 30 min. Subsequently, 1×10^4 cells were inoculated on each sample, and they were then incubated for a duration of 7 days. The growth medium was replaced every two days. To assess the viability of L929 cells and MC3T3 cells after 7 days of incubation, a Live/Dead viability kit (Thermo Fisher Scientific) was employed. A fluorescence microscope (EVOS FL, Thermo Fisher Scientific) was used to capture images. After obtaining eight Live/Dead images each for L929 and MC3T3 cells, the ratios of live cells to dead cells were calculated for each images using Image J(National Institute of Health).

Evaluation of cell attachment and infiltration

For cell attachment analysis, each sample was placed in a 12-well microplate and subjected to UV sterilization for 30 min. Subsequently, 1×10^4 L929 or MC3T3 cells were inoculated onto each sample and incubated for 7 days. The growth medium was replaced every two days. After incubation, the culture medium was aspirated, and the samples were washed twice with Dulbecco's Phosphate-Buffered Saline (DPBS, Gibco). Following the washes, a 4 % glutaraldehyde solution was added, and the samples were kept at 4 °C for 1 h. For dehydration, the cells were exposed to a series of graded ethanol concentration (25 %, 50 %, 75 % and 90 %) for 5 min at each step. Subsequently, the plates were dried overnight at room temperature. The cell attachment was analyzed using SEM.

For cell infiltration analysis, 1×10^4 L929 cells were inoculated onto each sample and incubated for 14 days. We followed the cell fixation protocol mentioned. We evaluated cell infiltration, on the side where L929 cells were seeded and on the opposite side.

Real time polymerase chain reaction analysis

Gene expression was assessed by real-time PCR. MC3T3 cells were seeded onto each membrane at a density of 1×10^4 cells and waited to attach for 4 h. Following attachment, cells were treated with a growth medium and incubated at 37 °*C* under a 5 % CO_2 atmosphere for 7 and 14 days. The growth medium was replaced every two days. Total RNA was isolated from each group using Trizol reagent ((Invitrogen Life Tech, Carsbad, CA, USA) and reverse transcribed into cDNA using Accupower cyclescipt RT premix & master mix (Bioneer, Daejun, Korea). Real-time PCR analysis was performed using SYBR premix Ex Taq II (Takarka Bio, Kusatsu, Japan) on a Real Time PCR system (StepOne Plus 3, Applied Biosystem, Foster City, CA, USA). The primers used in this study were osteocalcin (OCN), alkaline phosphatase (ALP), Runt-related transcription factor 2 (RUNX2) and glyceraldehyde 3 phosphate dehydrogenase (GAPDH) as listed in Table 2.

Statistical analysis

Statistical analysis was performed at $\alpha = 0.05$ level of significance and error bars in figures represented 95 % confidence interval. SPSS Statistics 23 (IBM, Armonk, NY, USA) was used for the statistical analysis. The Shapiro-wilk test was used to determine equal variance for all statistical data. One-way ANOVA was applied to these values. Turkey's HSD test was used for comparing multiple values.

Results

Transmission electron microscopy images of mineral trioxide aggregate

The TEM images presented in Fig. 1 illustrate the morphology of MTA. MTA particles were observed to have a size of approximately 200 nm (Fig. 1a). However, despite undergoing sonication procedures, MTA particles exhibited a tendency to aggregate, as observed in Fig. 1b and c.

Morphology, composition, and phase state of electrospun membrane

Morphology of electrospun membrane

Fig. 2a–f illustrates a comparison between the front and back sides of each membrane using SEM images. No significant differences in physical characteristics, such as fiber diameter and pore size, were observed. There was no noticeable pattern of fiber compression on the back side. Fig. 2g–i shows that the fiber diameter exhibited a normal distribution, with an average diameter of 2.03 μm for PCL, 2.21 μm for 2MTA, and 2.05 μm for 4 MTA. There was no statistical difference in fiber diameter among the membranes ($P > 0.05$).

Chemical composition and phase state of electrospun membrane

Fig. 3a, representing PCL, showed a composition composed of C and O. In Fig. 3b, 2MTA, the mass % of Ca and Zr was 1.84 % and 6.65 %, respectively. In Fig. 3c, 4MTA, the mass % of Ca and Zr was 3.47 % and 13.96 %, respectively. The mass % of Ca and Zr in 2MTA and 4MTA differed by approximately a factor of two. In Fig. 3d, PCL exhibited high crystallinity

Table 2 Sequence of forward (F) and reverse (R) primers for OCN, ALP, RUNX2, and GAPDH of MC3T3.

Primer name	Sequence	Reference
OCN _ F	5′-GCAATAAGGTAGTGAACA GACTCC	NM_007541
OCN _ R	5′-GCGTTTGTAGGCGGT CTTCAAG	
ALP _ F	5′-CCAGCAGGTTTCTCTCTTGG	NM_001271630
ALP _ R	5′-GGGATGGAGGAGAGAAGGTC	
RUNX2 _ F	5′-GCAGCACTCCATATCTCTACT	NM_007431
RUNX2 _ R	5′-TTCCGTCAGCGTCAACAC	
GAPDH _ F	5′-AAGGTCATCCCAGAGCTGAA	NM_008084.3
GAPDH _ R	5′-AGGAGACAACCTGGTCCTCA	

OCN; Osteocalcin, ALP; Alkaline phosphate, RUNX2; Runt-related transcription factor 2, GAPDH; Glyceraldehyde 3 phosphate dehydrogenase, MC3T3; Murine pre-osteoblast cells.

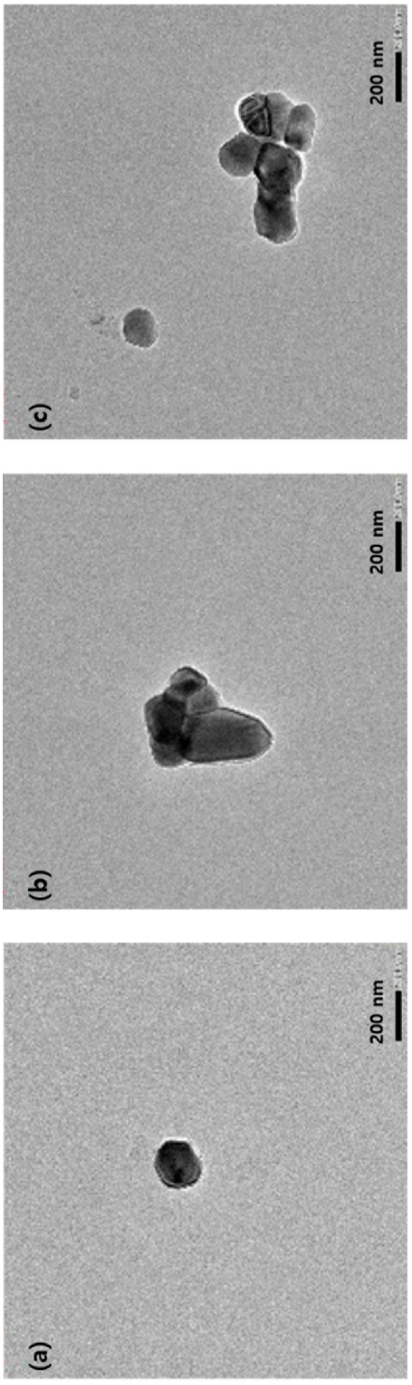

Fig. 1 Results of transmission electron microscopy (TEM) images of dispersed unhydrated mineral trioxide aggregate (MTA) particles. (a), The size of an individual MTA particle was approximately 200 nm. (b), Despite undergoing a dispersion process, it was not possible to completely prevent the aggregation of unhydrated MTA particles. (c), When multiple MTAs aggregated, they formed particles with a size of approximately 600 nm. The scale for all images shown was 200 nm.

as indicated by peaks at 21.5° and 23.8°. MTA, as shown in Fig. 3e, exhibited peaks corresponding to Zirconia (ZrO_2) and tricalcium silicate (C3S). These same peaks were also present in Fig. 3f–g. Notably, the peak intensity corresponding to PCL decreased in 4MTA compared to 2MTA and PCL, while the peak intensity associated with MTA increased.

Physicochemical properties of mineral trioxide aggregate embedded electrospun polycaprolactone membrane

Tensile strength test

In Fig. 4a shows that PCL, 2MTA, and 4MTA, all with identical dimensions, exhibited an elongation capacity of approximately 200 % along with similar Young's modulus values. In Fig. 4b, the tensile stress for each membrane is approximately 2.5 MPa, with no statistical difference observed ($P > 0.05$).

pH variance

Fig. 4c illustrates that PCL remained unaffected by changes in pH, while both 2MTA and 4MTA exhibited significant increases in pH. After 24 h of immersion, 2MTA reached a pH of 10.4 whereas 4MTA reached a pH of 11.2. A statistical difference was observed between 2MTA and 4MTA ($P < 0.05$).

Water contact angle

In Fig. 4d–e, the water contact angle of PCL was approximately 120°. Meanwhile, 2MTA measured around 115°, and 4MTA measured about 106°. A statistically significant difference in the water contact angle was observed between PCL and 4MTA. Importantly, there was no difference in wettability between the front and back sides of each membrane ($P > 0.05$). Therefore, the first null hypothesis is rejected.

Antimicrobial effect

The study employed *S. aureus* (ATCC 23235, Manassas, VA, USA) and *C. albicans* (ATCC 10231). *S. aureus* was cultured in brain heart infusion broth (BHI; BD Biosciences, Franklin Lakes, NJ, USA) and *C. albicans* was cultured in sabouraud dextrose broth (SD; MB cell, Seoul, Korea). In Fig. 5a–b, there was no statistical difference in bacterial viability between the control group and the PCL group ($P > 0.05$). However, as the concentration of MTA increased, there was a statistical significant decrease in *S.aureus* and *C.albicans* viability; specifically, 4MTA exhibited significantly lower viability compared to 2MTA ($P < 0.05$). The electrospun membrane containing MTA exhibited effectiveness against both bacteria and fungi. Therefore, the second null hypothesis is rejected.

Live/dead cell viability test

The viability of L929 and MC3T3 cells seeded on each membrane was evaluated over a 7-day period using Live/Dead cell imaging (Fig. 6). In Fig. 6a–d, L929 cells exhibited minimal dead cell presence. Similarly, in Fig. 6e–h, the number of dead MC3T3 cells observed did not differ significantly between the groups. In Fig. 6i, L929 cells

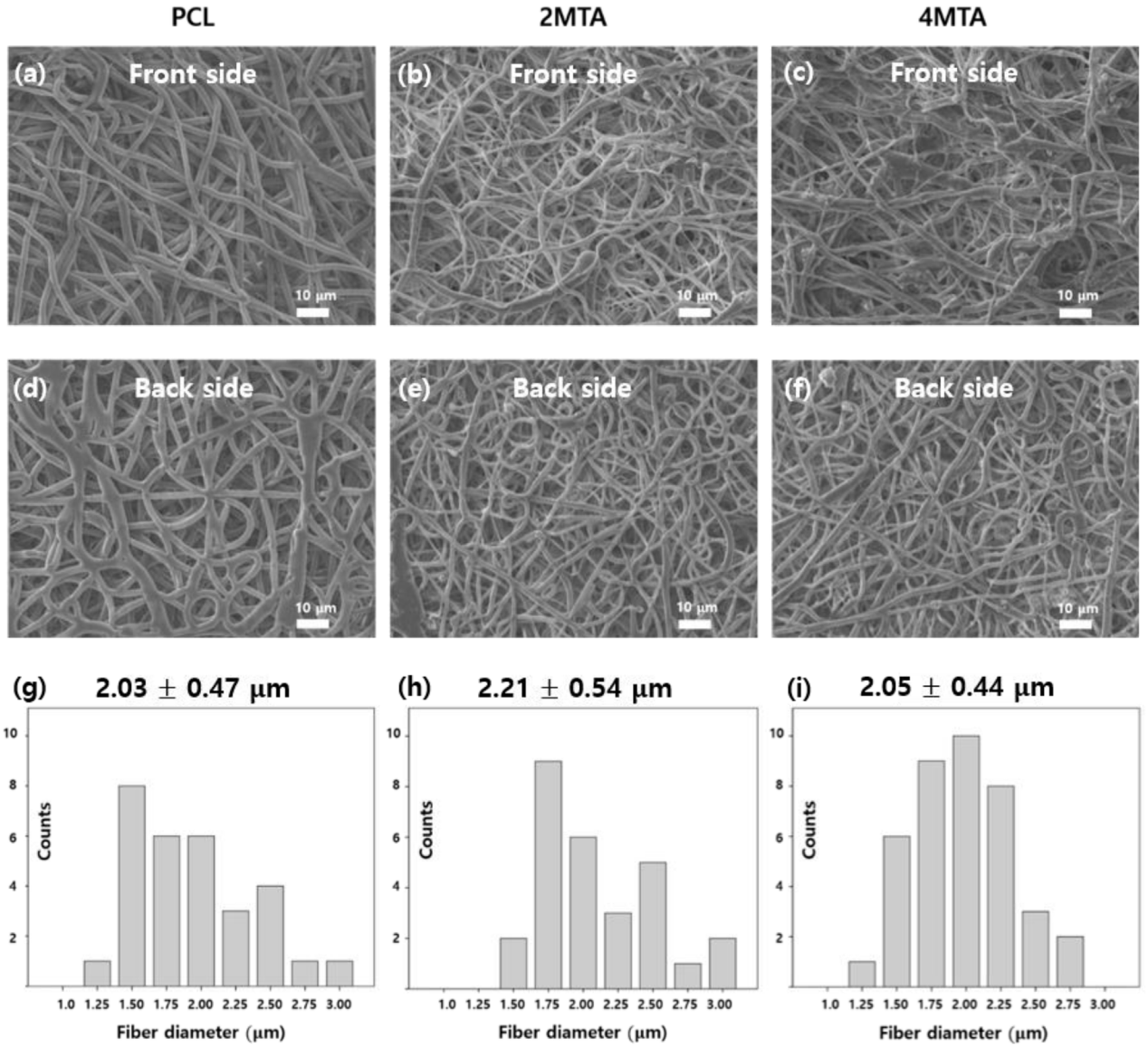

Fig. 2 (a–f), Scanning electron microscopy (SEM) images of both front and back sides of the electrospun membrane with a magnification of 1000x. The scale for all images shown was 10 μm. (a,d), Front and back side images of polycaprolactone (PCL). (b,e) Front and back side images of 2MTA. (c,f), Front and back side images of 4TMA. There was no difference between the two sides of each electrospun membrane. (g), The average fiber diameter of PCL was 2.03 ± 0.47 μm. (h), The average fiber diameter of 2MTA was 2.21 ± 0.47 μm. (i), The average fiber diameter of 4MTA was 2.05 ± 0.47 μm. Statistical analysis revealed no significant difference in fiber diameter among the membranes ($P > 0.05$).

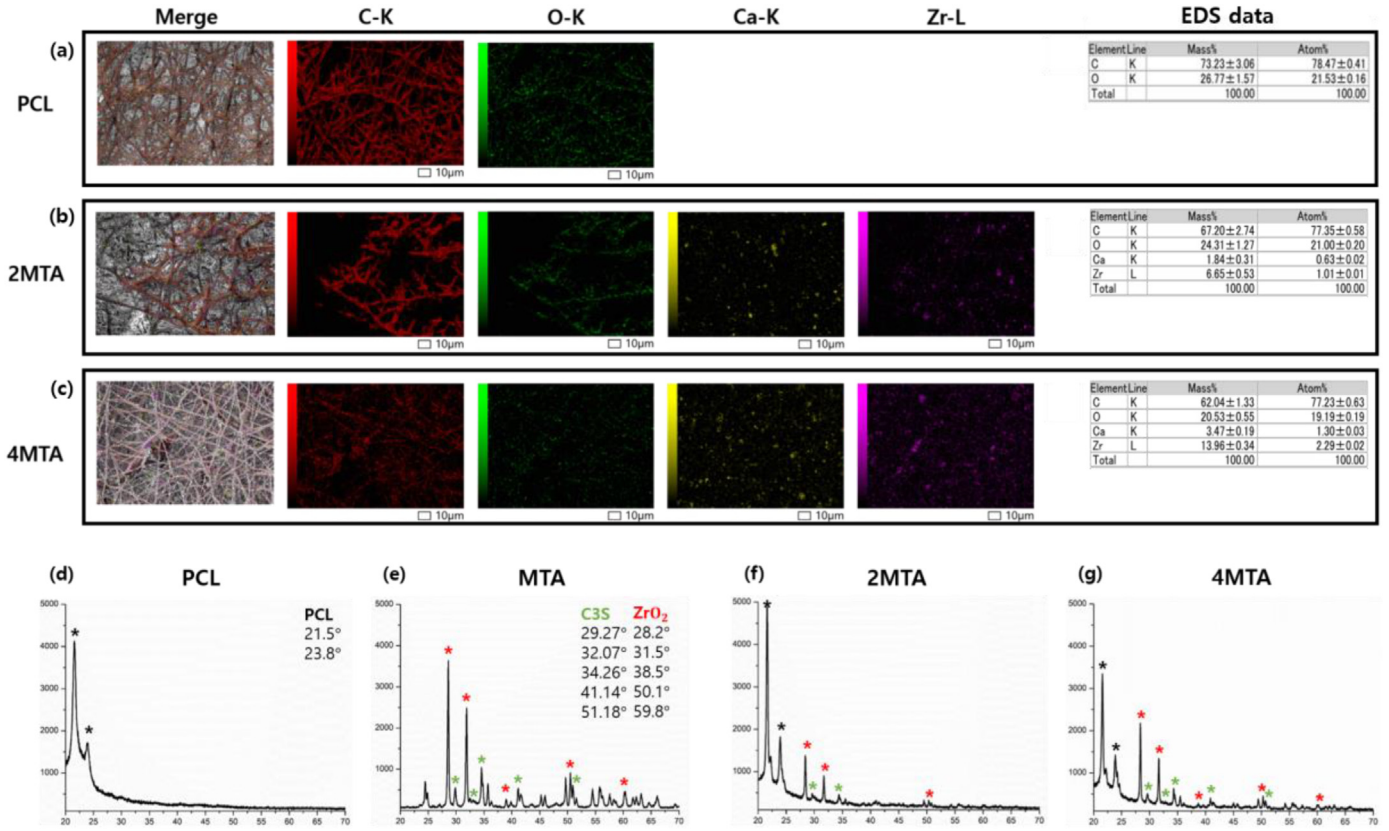

Fig. 3 The color code was as follows. Red: Carbon (C), Green: Oxygen (O), Yellow: Calcium (Ca), and Purple: Zirconium (Zr)/The scale for Fig. 3a–c images shown was 10 μm with a magnification of 1000x. (a–c), The mass % and atom % of the elements Ca and Zr increased proportionally with the increasing additive amount of mineral trioxide aggregate (MTA). (d–g), These x-ray diffraction (XRD) graphs represent each membrane. (d), Black asterisks(*) denoted polycaprolactone (PCL) peaks. (e), Green asterisks(*) represented tricalcium silicate (C3S) peaks, while red asterisks(*) indicated zirconium dioxide (ZrO^2) peaks. (f,g), Peaks corresponding to both PCL and MTA were observed. The 4MTA, which contained a higher MTA content, exhibited lower PCL peak intensity compared to 2MTA and higher ZrO_2 and C3S peak intensities.

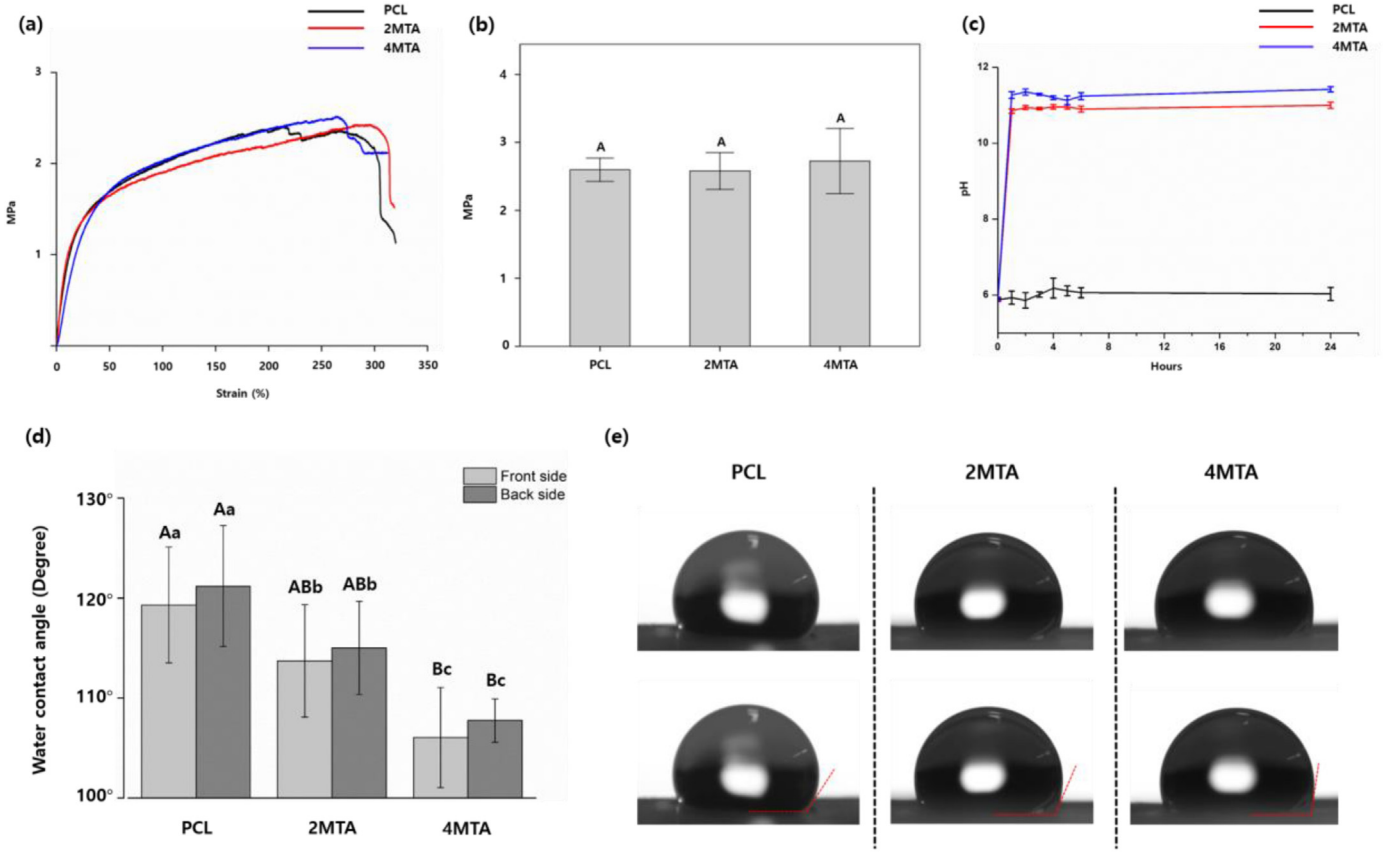

Fig. 4 (a), These graphs represented the typical stress-strain curves for each membrane. (b), Different capital letters denoted a statistical difference in tensile stress among the three groups. There was no statistically difference in tensile stress among the three groups ($P > 0.05$). (c), The graph depicted pH changes after 24 h of immersion in the membranes, revealing statistically significant differences among all three ($P < 0.05$). (d), These were the results for the water contact angle of each membrane. Different capital letters denoted statistical significant differences in water contact angles among different groups, while lowercase letters indicated statistical significant differences in water contact angles between the front and back side of the same group. Statistical decrease in the water contact angle were observed as the mineral trioxide aggregate (MTA) content increased ($P < 0.05$). Additionally, there is no statistical difference in water contact angle between the front and back sides. (e), These were representative images of distilled water on the membrane, and similar to Fig. 4d, they showed a decreasing tendency in contact angle.

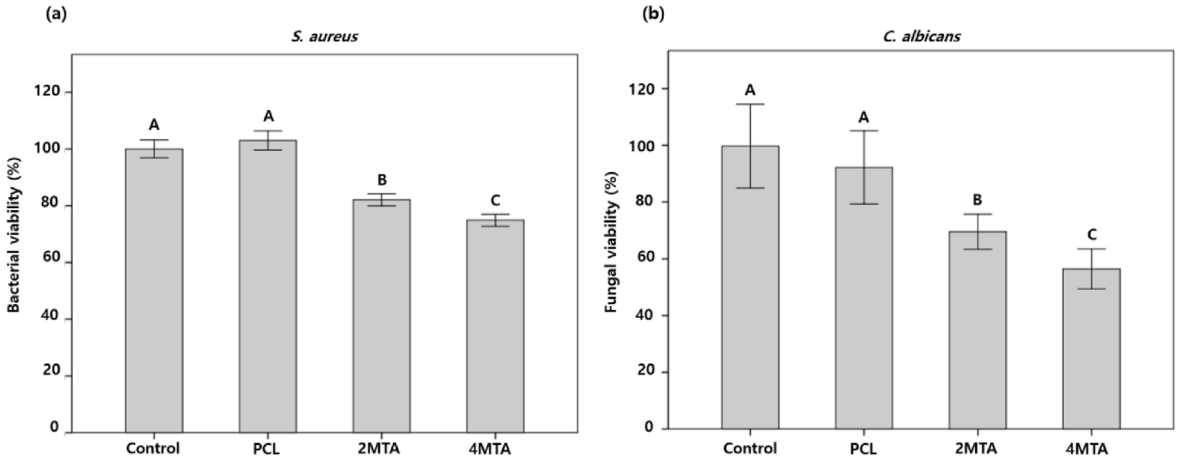

Fig. 5 Evaluation of bacterial and fungal viability using the MTT assay. Different capital letters denoted statistically significant differences in viability between each groups. (a), The polycaprolactone (PCL) groups did not show a significant decrease in bacterial viability compared to the control, while 2MTA and 4MTA demonstrated approximately 18 % and 25 % reductions in bacterial viability relative to the control group, respectively. Additionally, 4MTA exhibited the lowest bacterial viability ($P < 0.05$). (b), Similarly to (a), higher MTA concentrations were associated with lower fungal viability, while 2MTA and 4MTa demonstrated approximately 25 % and 40 % reductions in fungal viability relative to the control group, respectively. Also, 4MTA showed the lowest fungal viability ($P < 0.05$).

exhibited an approximately 80 % viable cell ratio across all groups, with no statistically significant differences observed among the groups ($P > 0.05$). Additionally, in Fig. 6j, the viable cell ratio for MC3T3 cells was approximately 90 % in all groups, and there were no statistically significant differences observed among the groups ($P > 0.05$). Therefore, it was determined that the electrospun membranes with embedded MTA did not impact the viability of fibroblast and pre-osteoblast cells.

Cell attachment and infiltration

In this study, the membrane was utilized as the reference point, dividing the experimental setup into two distinct regions: the oral side and the bone defect side. On the oral side, we assessed the attachment of L929 cells, while on the bone defect side, we evaluated the attachment of MC3T3 cells. Notably, in Fig. 7a–c, the morphology of the ECM was replicated, and cell attachment was observed, even on the most hydrophobic PCL membrane. Fig. 7b–c reveal that L929 cell attachment occurred in the 2MTA and 4MTA, similarly Fig. 6c–d. Additionally, Fig. 7d–f shows the attachment of MC3T3 cells to the surfaces of each respective group, with no significant difference in cell attachment observed among the groups.

L929 cells were cultured on the membrane for 14 days, and observations were made on both the sides where the cells were seeded and the opposite side in Fig. 7g-l. In Fig. 7g–i, a greater number of L929 cells were observed on the membrane compared to Fig. 7a–c. Furthermore, it was observed that L929 cells proliferated parallel to the surface of the membrane. However, in Fig. 7j-l, it was noted that each membrane prevented the infiltration of L929 cells, and as a result, L929 cells were not observed on the opposite side.

Real time polymerase chain reaction

Fig. 8 shows the changes in OCN, ALPand RUNX2 gene expression for each group relative to the control. In Fig. 8a, after 7 days, there was a significant increase in the gene expression of ALPand RUNX2 in the 2MTA and 4MTA, while the increase in OCN expression was relatively smaller. However, in Fig. 8b, after 14 days, there was a substantial increase in OCN expression, and the expression of RUNX2 decreased compared to day 7. When cultured with 4MTA, gene expression for all genes was statistically significant and highest at both 7 and 14 days ($P < 0.05$). Therefore, the third null hypothesis is rejected.

Discussion

The objective of this study is to transform MTA into a membranous structure to harness its inherent properties within a barrier membrane. We aimed to imbue synthetic polymer membranes with hydrophilic characteristics, antimicrobial properties, and osteogenic potential through straightforward integration of MTA. Furthermore, we evaluated one of the primary functions of barrier membranes, which is to prevent fibroblast infiltration.

When MTA in paste form undergoes hydration, its primary component, C3S, undergoes a transformation into calcium silicate hydrate (CSH) and calcium hydroxide ($CaOH_2$). This process fills the voids in MTA paste, resulting in a denser structure.[18–20] To preserve MTA in an unhydrated state and enhanced its dispersion, we combined MTA with organic solvents CF and DMF. Generally, $CaOH_2$ phase peaks were observed at 34.02° and 47.11°, but Fig. 3f–g did not show these peaks.[21] Hence, we can conclude that the manufactured membranes were in an unhydrated state.

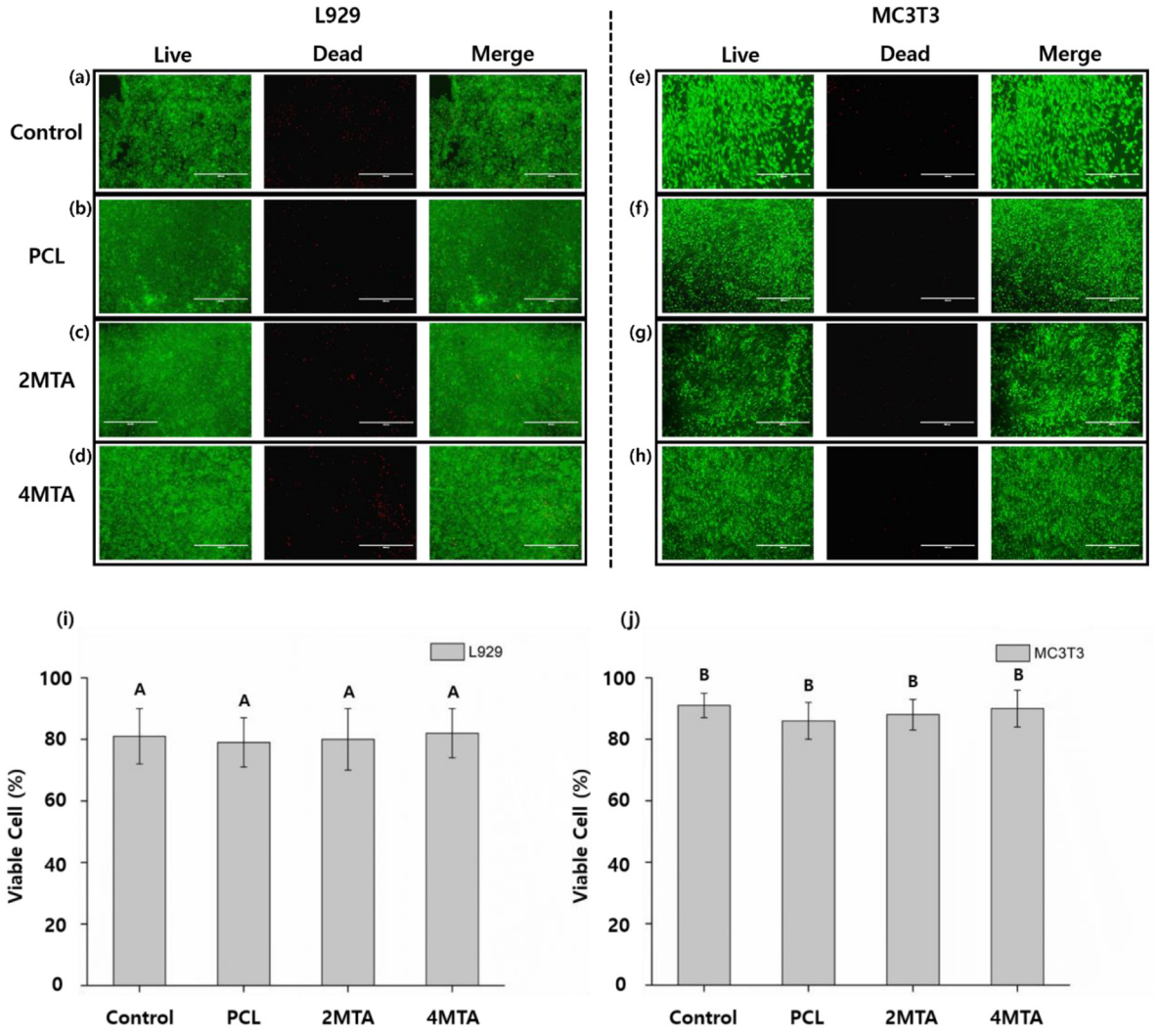

Fig. 6 Viability assessment of two cell types after 7 days of culture. The scale for Fig. 6a—h images shown was 400 μm. (a—d), These are a representative Live/Dead cell images of L929 cells, and there were no difference in proliferation and the number of dead cells between the groups. (e—h), These are a representative Live/Dead cell images of MC3T3 cells and a similar pattern of dead cells was observed regardless of the presence or absence of mineral trioxide aggregate (MTA). (i, j) The live cell and dead cell ratio of the Live/dead assay images was calculated using Image J program.

Subsequently, EDS data in Fig. 3b—c shows that Ca and Zr elements were uniformly distributed in the membrane, indicating the successful transformation of paste form MTA into membrane form MTA. Furthermore, when PCL with a M_w of 80,000 was electrospun at a rate of 1 mL/h for 30 min and then immersed in PBS for 12 weeks, a 50 % weight loss was observed.[22] Therefore, we expected that the 2MTA and 4MTA samples could be sufficiently degradable.

When operating parameters and environment conditions are held constant, the primary factor influencing electrospinning is the properties of the electrospinning fluid.[23] Variations in liquid viscosity and electrical conductivity may exist among PCL, 2MTA, and 4MTA suspension. It is known that liquid viscosity affects fiber diameter and uniformity, while electrical conductivity influences fiber diameter and distribution.[24—27] Additionally, as observed in Fig. 1a—c, the size of an unhydrated MTA agglomerate was approximately 200—600 nm. The average diameter of fibers in each group was approximately 2 μm. Furthermore, Fig. 4a—b demonstrated that the tensile strength (MPa), maximum strain (%), and elastic modulus values were consistent across all groups. Therefore, the addition of MTA did not impact the morphological and mechanical properties. It is important to note that Gelistilich's Bio-Gide, a xenogeneic barrier membrane known for having a similar dimension to the membrane used in this experiment, exhibited a tensile strength of 4—5 MPa and an elongation at break of 50 %.[28,29] Although the tensile strength of the PCL membrane with added MTA was only half that of Bio-Gide, its high maximum strain value suggested that it could be suitable for vertical bone augmentation where extension of the barrier is required.

As previously mentioned, the addition of MTA did not alter the morphological and mechanical characteristics. However, it impacted physicochemical properties such as pH and water contact angle. The weight of the membrane

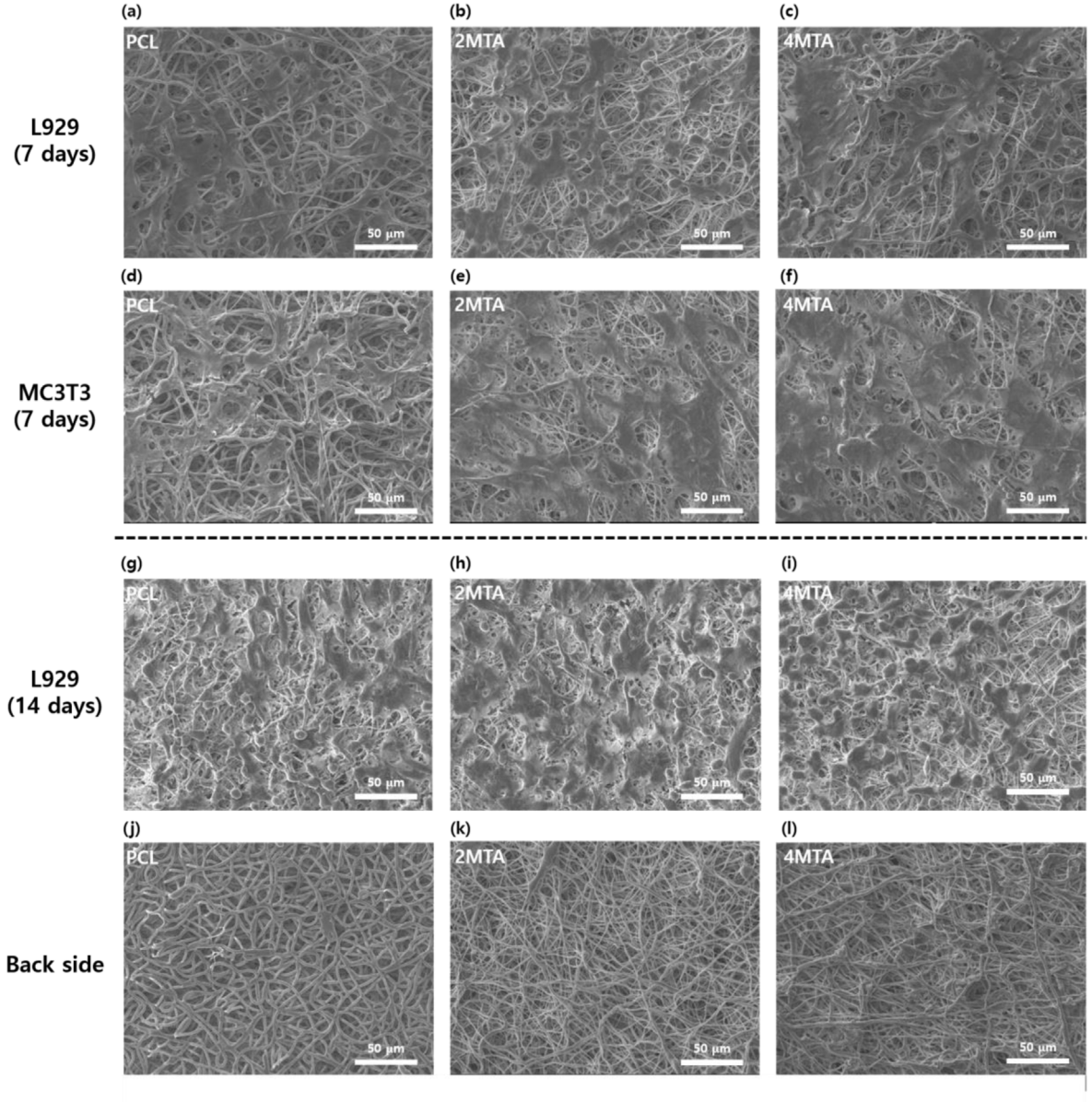

Fig. 7 The evaluation of cell attachment on both the oral and bone defect sides when using each membranes for guided bone regeneration (GBR). The scale for Fig. 7 images shown was 50 μm with a magnification of 500x. (a–c) After 7 days of culture, it was possible to observe the attachment of L929 cells (fibroblast) to each membrane. (d–f), Similarly, MC3T3 cells (preosteoblast) also attached to each membrane. (g–i), The evaluation of L929 cell infiltration (g–i), The proliferation of L929 cells on the membrane was observed. (j–l), Opposite side, L929 cells were not observed, indicating that the 0.4 mm thick membrane effectively prevented cell infiltration.

was 0.015 g, and mathematically, the amount of MTA included in the 2MTA was 0.002 g (two-fifteenths of 0.015 g), while in the 4MTA, it was 0.004 g (four-fifteenths of 0.015 g). Despite the small amount of MTA included, as shown in Fig. 4c, the pH values for 2MTA and 4MTA were 10.4 and 11.2, respectively. The reason for the increase in pH is that during the hydration process of C3S into CSH and $CaOH_2$, the OH^- ions from $CaOH_2$ raise the pH.[30] The ability to achieve a high pH level with a small amount of MTA can be attributed to the following factors: pH is influenced by the dispersion level of particles and the surface area to volume ratio.[31] The MTA particles in 2MTA and 4MTA produced through electrospinning were uniformly dispersed on a sub-micrometer scale and exhibited a high surface area to volume ratio, making the hydration reaction easier to occur. Due to this alkalinity, 2MTA and 4MTA were able to exhibit antimicrobial properties as illustrated in Fig. 5. Various microorganisms could lead to infections at GBR sites, with commonly observed pathogens being *S. aureus* and *C. albicans*.[32] It has been reported that these two pathogens, when exhibiting a synergistic effect, could lead to pathogen occurrence and drug resistance.[33] MTA has been shown to have an effect in reducing the viability of *S. aureus* and *C. albicans*, and this effect was also observed in this study.[34,35]

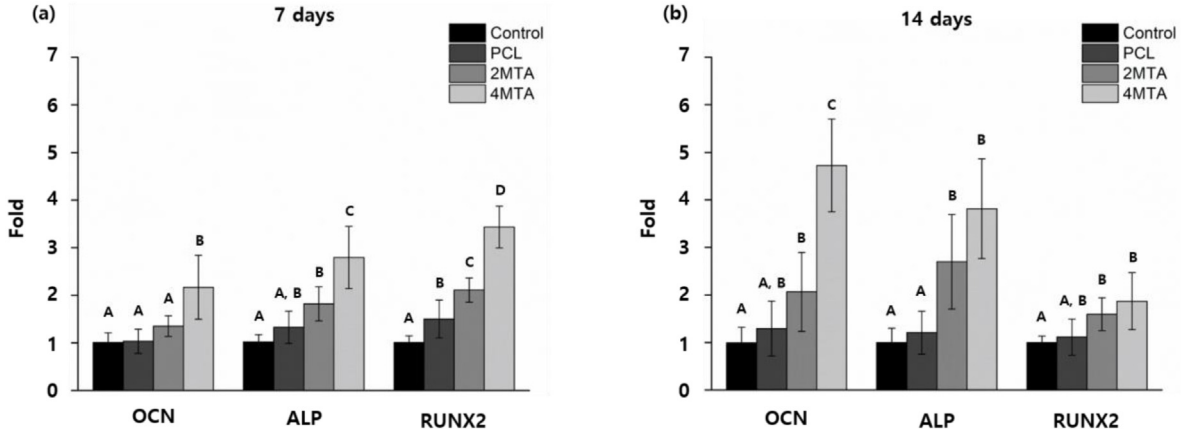

Fig. 8 The evaluation of changes in the gene expression of osteocalcin (OCN), alkaline phosphatase (ALP), and runt-related transcription factor 2 (RUNX2). Different capital letters denote statistically significant differences in the expression of each gene. (a), After 7 days, the gene expression levels of 4MTA increased the most significantly among all groups ($P < 0.05$), with RUNX2 showing the highest expression among the genes. (b), After 14 days, the gene expression levels of 4MTA increased the most significantly among all groups ($P < 0.05$), with OCN exhibiting the highest expression among the genes.

Another physicochemical property that varied with the MTA content was the water contact angle. PCL is inherently hydrophobic,[14] but MTA has a highly hydrophilic nature with a water contact angle of approximately 10—20°.[36] As a result, as shown in Fig. 4d—e, as the MTA content within the membrane increased, the water contact angle decreased. One of the considerations in this experiment was assessing whether the properties of the membrane's front and back sides were identical. The results, as seen in Fig. 2a—f, revealed that there was no difference in surface morphology between the front and back sides. Additionally, Fig. 4d—e demonstrated that there was no difference in water contact angle. Therefore, during microbial and cell tests, experiments could be conducted without distinction between the front and back sides.

When fibroblast and osteoblast were individually incubated with MTA for 96 h, previous research reported no significant difference in the proliferation rate between both cells.[37] Similarly, as observed in Fig. 6, when examining the 7-day direct contact viability of L929 and MC3T3 cells using Live/Dead images, both cells showed proliferation, and there was no significant difference in the number of dead cells between the groups. The adequate evaporation of the organic solvent CF and DMF during the electrospinning process indicated that the membrane was biocompatible with both oral side cells (L292) and bone defect side cells (MC3T3). Furthermore, because cell attachment tends to increase with a lower water contact angle and a charged surface,[38] it was anticipated that there would be a significant increase in cell attachment in 4MTA. However, Fig. 7a—f exhibited minimal changes in cell attachment patterns among the groups because the average water contact angle difference between 4MTA and PCL was only about 10°, and it is expected that the surface charge modification by MTA was relatively weak.

The pore size that can effectively impede cell migration is typically 1 μm or less [39]. However, this refers to a two-dimensional case, specifically a single layer. In Fig. 7, the observed pore size of the electrospun membrane was approximately 10 μm. However, due to the three-dimensional internal space of the membrane being filled with numerous fibers, it was practically difficult for fibroblast infiltration to occur. Similarly, in Fig. 7g—f, L929 cells proliferated parallel to the membrane surface but did not penetrate to the opposite side, as could be observed in Fig. 7j-l.

MTA is known to upregulate the Jun N-terminal kinase (JNK) and extracellular regulated protein kinase (EPK) pathways in cells, leading to an increase in the expression of odontogenic-related genes such as OCN, ALP, and RUNX2.[40] In Fig. 8, when culturing cells with 4MTA for 7 and 14 days, it was evident that the expression levels of all gene types increased. In Fig. 8a, there was a dominant increase in the expression of ALP and RUNX2, while in Fig. 8b, OCN expression dominantly increased. Generally, considering that ALP and RUNX2 are early expression genes, and OCN is a late expression gene.[41] Fig. 8a—b exhibited a similar trend in gene expression increase. One noteworthy point is that it has been reported that it has been reported that the morphology of electrospun membranes can influence cell gene expression.[42] However, there was no statistically difference in gene expression between PCL and Control in ($P > 0.05$). Nevertheless, 2MTA and 4MTA showed statistical significant increases in gene expression compared to Control ($P < 0.05$), confirming that the increase in OCN, ALP, and RUNX2 expression was attributed to MTA. Consequently, it is anticipated that the use of 4MTA as a barrier membrane can aid in the regeneration of bone defects.

In this study, we have proposed a unique and novel barrier membrane; nonetheless, there are several limitations to consider. Firstly, we did not assess the degradation rate within each experimental group. Generally, PCL degrades through hydrolysis reaction.[43] While 2MTA and 4MTA demonstrated increased hydrophilicity compared to PCL, implying an anticipated acceleration in the degradation rate, we did not directly compare the actual rates of degradation. Secondly, all experiments were conducted *in vitro*, precluding the observation of potential tissue

responses that might occur when used *in vivo*. Despite these limitations, according to previous studies, electrospun membranes incorporating various substances such as bioceramic or medication have demonstrated the ability to maintain the existing characteristics *in vivo*.[44,45] Additionally, this represented the initial attempt to transform MTA into a membrane form for use as a barrier membrane. Future research initiatives should be directed towards the continued advancement of MTA in membrane form as a synthetic barrier membrane with the potential to supplant xenogeneic barrier membranes.

Declaration of competing interest

The authors deny any conflicts of interest related to this study.

Acknowledgements

This work was supported by the Korea Medical Device Development Fund grant funded by the Korea government (the Ministry of Science and ICT the Ministry of Trade, Industry and Energy, the Ministry of Health & Welfare, the Ministry of Food and Drug Safety) (Project Number: 1711194220, RS_2020_KD000045).

References

1. Parirokh M, Torabinejad M. Mineral trioxide aggregate: a comprehensive literature eeview—art I: chemical, physical, and antibacterial properties. *J Endod* 2010;36:16—27.
2. Chiu YC, Fang HY, Hsu TT, Lin CY, Shie MY. The characteristics of mineral trioxide aggregate/polycaprolactone 3-dimensional scaffold with osteogenesis properties for tissue regeneration. *J Endod* 2017;43:923—9.
3. Baek SH, Lee WC, Setzer FC, Kim S. Periapical bone regeneration after endodontic microsurgery with three different root-end filling materials: amalgam, SuperEBA, and mineral trioxide aggregate. *J Endod* 2010;36:1323—5.
4. ElReash AA, Hamama H, Eldars W, Lingwei G, Zaen El-Din AM, Xiaoli X. Antimicrobial activity and pH measurement of calcium silicate cements versus new bioactive resin composite restorative material. *BMC Oral Health* 2019;19:1—10.
5. Kim Y, Lee D, Kye M, Ha YJ, Kim SY. Biocompatible properties and mineralization potential of premixed calcium silicate-based cements and fast-set calcium silicate-based cements on human bone marrow-derived mesenchymal stem cells. *Materials* 2022;15:7595.
6. Bottino MC, Thomas V, Schmidt G, et al. Recent advances in the development of GTR/GBR membranes for periodontal regeneration—a materials perspective. *Dent Mater* 2012;28:703—21.
7. Dimitriou R, Mataliotakis GI, Calori GM, Giannoudis PV. The role of barrier membranes for guided bone regeneration and restoration of large bone defects: current experimental and clinical evidence. *BMC Med* 2012;10:1—24.
8. Omar O, Elgali I, Dahlin C, Thomsen P. Barrier membranes. More than the barrier effect? *J Clin Periodontol* 2019;46:103—23.
9. Campoccia D, Montanaro L, Arciola CR. A review of the clinical implications of anti-infective biomaterials and infection-resistant surfaces. *Biomaterials* 2013;34:8018—29.
10. Cui W, Zhou Y, Chang J. Electrospun nanofibrous materials for tissue engineering and drug delivery. *Sci Technol Adv Mater* 2010;11:014108.
11. Mochane MJ, Motsoeneng TS, Sadiku ER, Mokhena TC, Sefadi JS. Morphology and properties of electrospun PCL and its composites for medical applications: a mini review. *Appl Sci* 2019;9:2205.
12. Je Jeon H, Lee H, Kim G. A surface-modified poly(ε-caprolactone) scaffold comprising variable nanosized surface-roughness using a plasma treatment. *Tissue Eng C Methods* 2014;20:951—63.
13. Shu Z, Zhang C, Yan L, et al. Antibacterial and osteoconductive polycaprolactone/polylactic acid/nano-hydroxyapatite/Cu@ZIF-8 GBR membrane with asymmetric porous structure. *Int J Biol Macromol* 2023;224:1040—51.
14. S Shi R, Huang Y, Zhang J, et al. Effective delivery of mitomycin-C and meloxicam by double-layer electrospun membranes for the prevention of epidural adhesions. *J Biomed Mater Res Part B: Appl Biomater* 2020;108:353—66.
15. Grela E, Kozłowska J, Grabowiecka A. Current methodology of MTT assay in bacteria—A review. *Acta Histochem* 2018;120:303—11.
16. Benov L. Improved formazan dissolution for bacterial MTT assay. *Microbiol Spectr* 2021;9:e01637. 21.
17. Kuhn D, Balkis M, Chandra J, Mukherjee P, Ghannoum M. Uses and limitations of the XTT assay in studies of Candida growth and metabolism. *J Clin Microbiol* 2003;41:506—8.
18. Camilleri J. Characterization and hydration kinetics of tricalcium silicate cement for use as a dental biomaterial. *Dent Mater* 2011;27:836—44.
19. Camilleri J, Cutajar A, Mallia B. Hydration characteristics of zirconium oxide replaced Portland cement for use as a root-end filling material. *Dent Mater* 2011;27:845—54.
20. Camilleri J. Characterization of hydration products of mineral trioxide aggregate. *Int Endod J* 2008;41:408—17.
21. Jiménez-Sánchez MdC, Segura-Egea JJ, Díaz-Cuenca A. Higher hydration performance and bioactive response of the new endodontic bioactive cement MTA HP repair compared with ProRoot MTA white and NeoMTA plus. *J Biomed Mater Res Part B: Appl Biomater* 2019;107:2109—20.
22. B Bazgir M, Zhang W, Zhang X, et al. Degradation and characterisation of electrospun polycaprolactone (PCL) and poly(lactic-co-glycolic acid) (PLGA) scaffolds for vascular tissue engineering. *Materials* 2021;14:4773.
23. Liu H, Gough CR, Deng Q, Gu Z, Wang F, Hu X. Recent advances in electrospun sustainable composites for biomedical, environmental, energy, and packaging applications. *Int J Mol Sci* 2020;21:4019.
24. Chowdhury M, Stylios G. Effect of experimental parameters on the morphology of electrospun nylon 6 fibres. *Int J Basic Appl Sci* 2010;10:70—8.
25. Prabu G, Dhurai B. A novel profiled multi-pin electrospinning system for nanofiber production and encapsulation of nanoparticles into nanofibers. *Sci Rep* 2020;10:4302.
26. Kara HH, Xiao F, Sarker M, et al. Antibacterial poly (lactic acid)(PLA) films grafted with electrospun PLA/allyl isothiocyanate fibers for food packaging. *J Appl Polym Sci* 2016;133:42475.
27. Wang S, Zhao X, Yin X, Yu J, Ding B. Electret polyvinylidene fluoride nanofibers hybridized by polytetrafluoroethylene nanoparticles for high-efficiency air filtration. *ACS Appl Mater Interfaces* 2016;8:23985—94.
28. Raz P, Brosh T, Ronen G, Tal H. Tensile properties of three selected collagen membranes. *BioMed Res Int* 2019;2019:5163603.
29. Q Qiu YL, Chen X, Hou YL, et al. Characterization of different biodegradable scaffolds in tissue engineering. *Mol Med Rep* 2019;19:4043—56.

30. De Moura AA, Effting L, Moisés MP, et al. The influence of calcium-rich environments in siliceous industrial residues on the hydration reaction of cementitious mixtures. *J Clean Prod* 2019;225:152—62.
31. Yang F, Niu Q, Lan Q, Sun D. Effect of dispersion pH on the formation and stability of Pickering emulsions stabilized by layered double hydroxides particles. *J Colloid Interface Sci* 2007;306:285—95.
32. Kamiński B, Błochowiak K, Kołomański K, Sikora M, Karwan S, Chlubek D. Oral and maxillofacial infections-A bacterial and clinical cross-section. *J Clin Med* 2022;11:2731.
33. Hu Y, Niu Y, Ye X, et al. Staphylococcus aureus synergized with candida albicans to increase the pathogenesis and drug resistance in cutaneous abscess and peritonitis murine models. *Pathogens* 2021;10:1036.
34. Mohammadi Z, Giardino L, Palazzi F, Shalavi S. Antibacterial activity of a new mineral trioxide aggregate-based root canal sealer. *Int Dent J* 2012;62:70—3.
35. Al-Hezaimi K, Al-Hamdan K, Naghshbandi J, Oglesby S, Simon JH, Rotstein I. Effect of white-colored mineral trioxide aggregate in different concentrations on candida albicans in vitro. *J Endod* 2005;31:684—6.
36. Ashi T, Mancino D, Hardan L, et al. Physicochemical and antibacterial properties of bioactive retrograde filling materials. *Bioeng* 2022;9:624.
37. Willershausen I, Wolf T, Kasaj A, Weyer V, Willershausen B, Marroquin BB. Influence of a bioceramic root end material and mineral trioxide aggregates on fibroblasts and osteoblasts. *Arch Oral Biol* 2013;58:1232—7.
38. Ferrari M, Cirisano F, Morán MC. Mammalian cell behavior on hydrophobic substrates: influence of surface properties. *Colloids Interfaces* 2019;3:48.
39. Bružauskaitė I, Bironaitė D, Bagdonas E, Bernotienė E. Scaffolds and cells for tissue regeneration: different scaffold pore sizes different cell effects. *Cytotechnology* 2016;68:355—69.
40. Du J, Lu Y, Song M, et al. Effects of ERK/p38 MAPKs signaling pathways on MTA-mediated osteo/odontogenic differentiation of stem cells from apical papilla: a vitro study. *BMC Oral Health* 2020;20:50.
41. Chung MT, Liu C, Hyun JS, et al. CD90 (Thy-1)-positive selection enhances osteogenic capacity of human adipose-derived stromal cells. *Tissue Eng Part A* 2013;19:989—97.
42. Chen Cy, Long S, Liu Z, et al. Effects of electrospun membrane surface morphology on cellular behaviours and osteogenesis of bone marrow mesenchymal stem cells. *Mater Res Express* 2023;10:065005.
43. Hakkarainen M. Aliphatic polyesters: abiotic and biotic degradation and degradation products. *Degradable Aliphatic Polyesters* 2002;157:113—38.
44. Shi R, Xue J, He M, Chen D, Zhang L, Tian W. Structure, physical properties, biocompatibility and in vitro/vivo degradation behavior of anti-infective polycaprolactone-based electrospun membranes for guided tissue/bone regeneration. *Polym Degrad Stabil* 2014;109:293—306.
45. da Fonseca GF, Avelino SdOM, Mello DdCR, et al. Scaffolds of PCL combined to bioglass: synthesis, characterization and biological performance. *J Mater Sci* 2020;31:1—10.